Marine Chemistry 158 (2014) 17–26

Contents lists available at ScienceDirect

Marine Chemistry

journal homepage: www.elsevier.com/locate/marchem

Source and distribution of glycerol dialkyl glycerol tetraethers along lower Yellow River-estuary–coast transect

Weichao Wu [a], Jiaping Ruan [a], Su Ding [a], Liang Zhao [a], Yunping Xu [a,b,*], Huan Yang [c], Weihua Ding [c], Yandong Pei [d]

[a] MOE Key Laboratory for Earth Surface Process, College of Urban and Environmental Sciences, Peking University, Beijing 100871, China
[b] Qingdao Collaborative Innovation Center of Marine Science and Technology, Qingdao 266003, China
[c] State Key Laboratory of Biogeology and Environmental Geology, China University of Geosciences, Wuhan 430074, China
[d] Tianjin Center, China Geological Survey, Tianjin 300170, China

ARTICLE INFO

Article history:
Received 7 June 2013
Received in revised form 22 October 2013
Accepted 8 November 2013
Available online 20 November 2013

Keywords:
Organic carbon
Yellow River
GDGTs
BIT
TEX_{86}

ABSTRACT

To assess the source of glycerol dialkyl glycerol tetraethers (GDGTs) and their usefulness as proxies for terrestrial organic matter inputs and temperature in the Yellow River-dominated margin, we measured isoprenoid and branched GDGT concentrations in surface sediments along a lower Yellow River-estuary–coast transect. Branched GDGTs dominated over isoprenoid GDGTs in the riverbed sediments and had similar compositions from river to coast. In contrast, isoprenoid GDGTs displayed an increasing abundance and a decreasing GDGT-0 to crenarchaeol ratio (1.6 to 0.6) toward the sea. Such distribution patterns of GDGTs, combined with the result from a principal component analysis (PCA), confirmed the different origin of branched and isoprenoid GDGTs with branched GDGTs being primarily from soil erosion of the Chinese loess plateau (CLP) whereas, in addition to allochthonous terrestrial inputs, aquatic Thaumarchaeota partially contributes to the isoprenoid GDGT pool in estuarine and coastal areas. The branched GDGT-derived temperature (avg. 11 °C) is consistent with the annual mean air temperature (MAT) of the CLP in the middle river basin, a major source region for the Yellow River sediments, whereas the isoprenoid-derived temperature (12.7 to 28.4 °C) deviated widely from the annual mean temperature in the study region. Application of a binary mixing model based on $\delta^{13}C$, the branched and isoprenoid tetraether (BIT) index and branched GDGT concentrations showed consistent decreases in the relative amount of terrestrial organic carbon toward the sea, but estimates from the latter two proxies were lower than those from the $\delta^{13}C$.

1. Introduction

Over the past decade, several geochemical proxies of organic carbon sources, temperature and soil pH based on the distribution of glycerol dialkyl glycerol tetraethers (GDGTs; Fig. 1) have been proposed and increasingly applied to biogeochemical and paleo-environmental studies (Schouten et al., 2013 and references therein). These proxies include the TEX_{86} (TetraEther indeX of 86 carbon atoms) (Schouten et al., 2002), MBT/CBT (methylation index/cyclization index of branched tetraethers) (Weijers et al., 2007a) and BIT (branched and isoprenoid tetraether) indices (Hopmans et al., 2004). The TEX_{86} proxy is based on the relative abundance of isoprenoid GDGTs (*i*GDGTs) which are membrane lipids of Thaumarchaeota, formerly assigned to Crenarchaeota (Schouten et al., 2002; Sinninghe Damsté et al., 2002). Since the number of cyclopentane groups in Thaumarchaeotal *i*GDGT is primarily controlled by growth temperature, the TEX_{86} accumulated in sediments can be used to reconstruct sea (lake) surface temperature (e.g., Kim et al., 2008, 2010; Powers et al., 2010; Schouten et al., 2002). In contrast to *i*GDGTs, branched GDGTs (*b*GDGTs) are mainly produced by as-yet unknown anaerobic bacteria thriving in soil and peat, possibly belonging to the group of Acidobacteria (Hopmans et al., 2004; Sinninghe Damsté et al., 2011). By examining 134 soil samples from 90 globally-distributed locations, Weijers et al. (2007a) found that the MBT proxy was dependent on annual mean air temperature (MAT) and to a lesser extent on soil pH, whereas the CBT proxy is correlated with soil pH. Subsequent studies extended the soil dataset to 278 globally-distributed soils, and proposed new transfer functions for the reconstruction of soil pH and MAT (Peterse et al., 2012). Because soils are more widespread than peat in the terrestrial realm, the occurrence of *b*GDGTs in aquatic environments (e.g., lakes and marginal seas) was usually attributed to allochthonous inputs of soil organic matter via runoff (Hopmans et al., 2004). A global survey shows that the BIT index is generally higher than 0.9 in soil/peat and close to 0 in marine environments devoid of terrestrial inputs (Hopmans et al., 2004; Weijers et al., 2006b),

* Corresponding author at: MOE Key Laboratory for Earth Surface Process, College of Urban and Environmental Sciences, Peking University, Beijing 100871, China. Tel.: +86 10 62752091.
E-mail address: yunpingxu@pku.edu.cn (Y. Xu).

0304-4203/$ – see front matter © 2013 Elsevier B.V. All rights reserved.
http://dx.doi.org/10.1016/j.marchem.2013.11.006

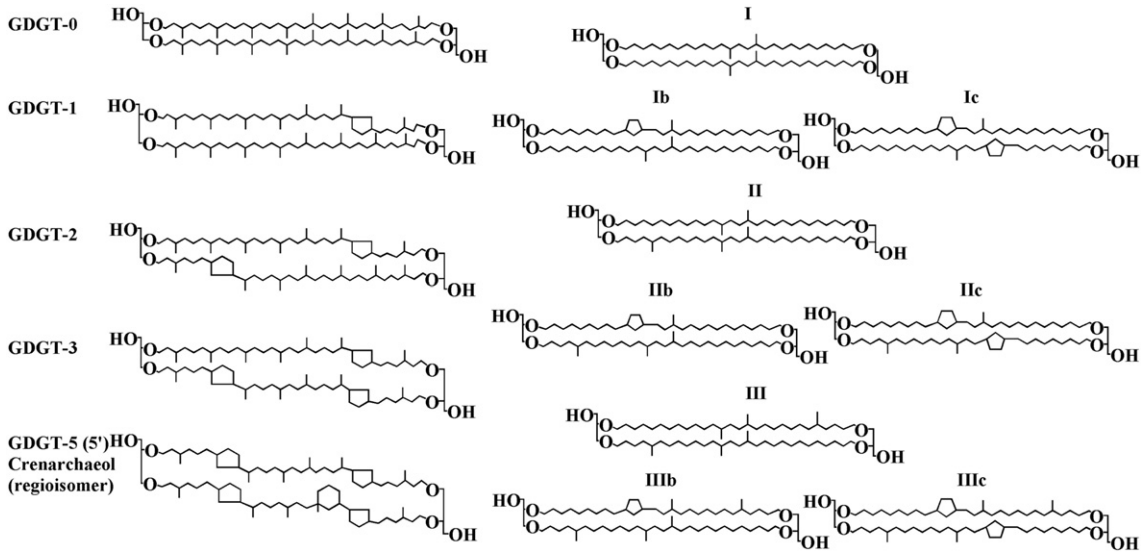

Fig. 1. Structures of isoprenoid and branched GDGTs. GDGT-5′ is a regioisomer of crenarchaeol with an anti-parallel configuration of the two glycerol moieties.

although some alkaline soils have exceptionally low BIT values (<0.3) (Yang et al., 2012).

Despite successful applications of GDGT-proxies (Schouten et al., 2013 and references therein), caution still should be taken. In-situ production of *b*GDGTs in lakes and rivers complicates the interpretation of the MBT/CBT and BIT indices as continental environmental proxies (Bechtel et al., 2010; Blaga et al., 2010; Tierney et al., 2012; Zell et al., 2013; Zhu et al., 2011). On the other hand, significant inputs of terrestrial *i*GDGTs can bias the TEX_{86}-derived temperature signal in marginal seas or small lakes (Powers et al., 2010; Weijers et al., 2006a). Thus, it is crucial to elucidate the origins of *b*GDGTs and *i*GDGTs before they can be confidently used as environmental proxies.

River-dominated continental margins are subject to the intensive land–ocean interactions. Because of large terrestrial inputs and relatively high primary productivity, river-dominated continental margins play a key role in the global carbon cycle, and their sediments contain abundant information about marine and continental environments (Pancost and Boot, 2004). Previous studies of the Amazon (Kim et al., 2012; Zell et al., 2013), the Yangtze (Yang et al., 2013; Zhu et al., 2011) and the Mississippi Rivers (Smith et al., 2012) have identified multiple sources of GDGTs and complex processes in river systems. Compared to other large rivers, the Yellow River (YR) is distinguished by its extremely high turbidity with suspended particle loads of up to 220 kg m^{-3} (Ren and Shi, 1986), and may have unique microbial community and biogeochemical behaviors. Nevertheless, so far no data is available for GDGTs in the YR, although limited studies have focused on the BIT index in its adjacent seas (Wu et al., 2013; Zhao et al., 2011).

Here, we present a comprehensive study about the distributions and compositions of GDGTs in surface sediments along a lower YR-estuary–coast transect. Our main aims are to: (1) constrain sources of *b*GDGTs and *i*GDGTs by comparing soils in the Chinese loess plateau (CLP), a principal contributor to the YR sediments (Ren, 2006); and (2) evaluate the applicability of the GDGT-based proxies in the YR-dominated continental margin.

2. Materials and methods

2.1. Study area and sampling

The YR with a total length of 5464 km drains a wide basin that covers over 750,000 km^2 of China (Wang et al., 2007). It originates in the Bayankala Mountains of the Tibet Plateau (western China), flows through nine provinces and discharges into the Bohai Sea (northeastern China). The upper, middle and lower YR basins have distinct climates with MATs of 1 to 4 °C, 8 to 14 °C, and 12 to 14 °C, respectively (Chen et al., 2005) and mean annual precipitations of 368 mm, 530 mm and 670 mm, respectively (IRTCES, 2004). Due to severe soil erosion in the CLP in the middle river basin, the YR has an annual sediment load of 1.1×10^9 ton, ranking as the world's second largest river in terms of sediment load (Milliman et al., 1987). The pattern of a sediment dispersal off the YR mouth is mainly controlled by the tidal shear fronts and the tidal currents (Bi et al., 2010). Because of the barrier effect of the tidal shear front and the weak river flow, most sediment from the YR is deposited near the estuary and in the adjacent sea, causing the YR delta to grow at a rate of approximately 1.29 km per year (Li et al., 2001; Wang et al., 2007). The modern YR delta, with an area of 5400 km^2, formed after 1855 when the YR started to drain into the Bohai Sea (Pang and Si, 1979).

In July 2011, a total of forty surface sediments (0–10 cm) were collected by a grab sampler. These samples can be divided into four groups, namely the lower YR, the modern YR estuary (1996–present), the old YR estuary (1976–1996) and the coast (Fig. 2). They are dominated by silt (avg. 61.1%), fine sand (avg. 28.9%) and clay (avg. 9.9%). In addition, fifty surface soil samples (0–2 cm) were collected over an extensive area of the CLP (latitude from 32°N to 42°N; longitude from 100°E to 120°E) in order to compare their geochemical properties to those of the sediments in the YR-dominated continental margin. The soils in the CLP developed on clastic, predominantly silt-sized wind-blown sediment and include various soil types such as cultivated loessial soil and dark loessial soil. After collection, all samples were stored at −20 °C until analysis.

2.2. Grain size, elemental and stable isotope analyses

For grain size analysis, freeze-dried sediments were reacted with excess 1 N hydrochloric acid and hydrogen peroxide to remove carbonates and decompose the organic matter, respectively (Sun et al., 2011). After that, sodium hexametaphosphate [$Na(PO_3)_6$] was added, and the sediments were allowed to settle for 24 h. After ultrasonication for 1 min, the sediment grain size was measured by a Mastersizer 2000 Laser Particle Size Analyzer. The scan range was from 0.02 to 2000 μm, and categorized into three fractions: sand (64–2000 μm), silt (4–64 μm) and clay (<4 μm).

The elemental and stable isotopic analyses were described in detail by Sun et al. (2011). Briefly, excess 1 N hydrochloric acid was added

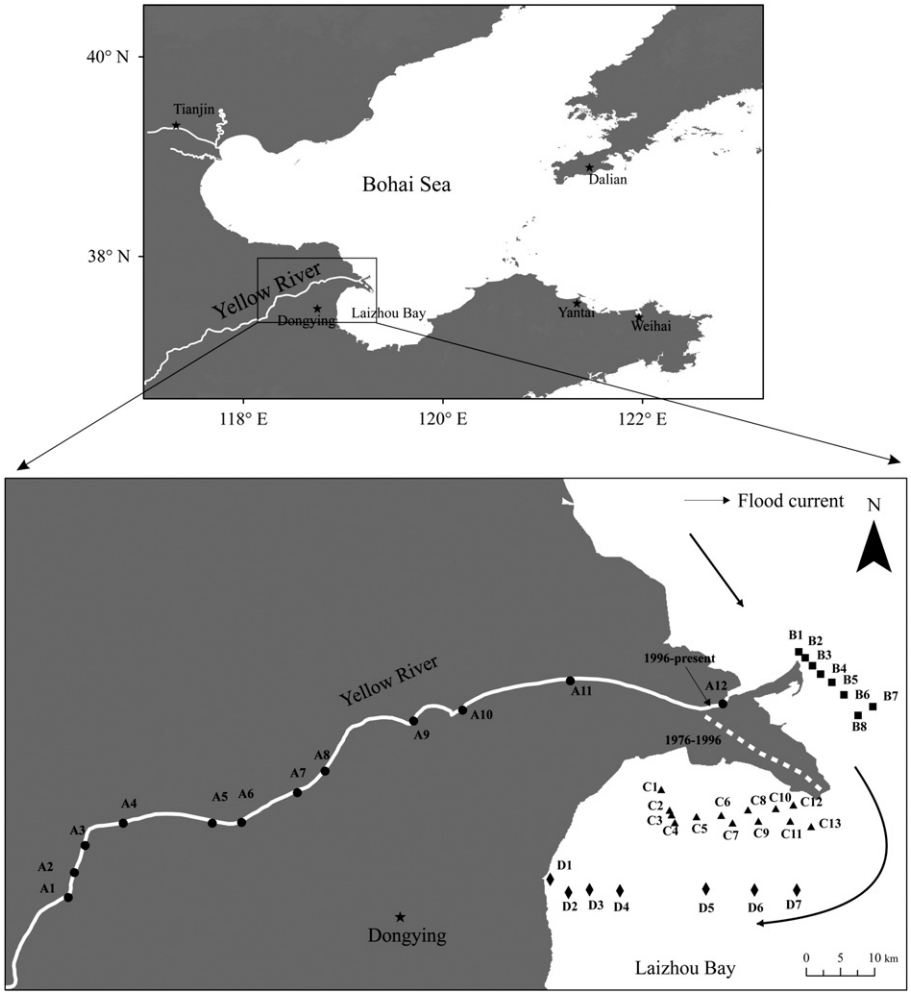

Fig. 2. Sampling sites for surface sediments in the Yellow River dominated continental margin: lower Yellow River reach (dot), modern estuary (square), old estuary (triangle) and coast (diamond). Dashed line represents the Yellow River channel of 1977–1996. The arrows show the suspended sediment dispersal pattern of the present Yellow River subdelta during the flood tidal phase.
Bi et al. (2010).

to the sediment to remove inorganic carbon. The sediment residue was rinsed with ultra-pure water until the solution pH was nearly neutral, and dried at 45 °C. Organic carbon (OC) and nitrogen (N) contents were determined with a CHNOS Elemental Analyzer (Elementar, Germany), whereas the $\delta^{13}C$ values were measured with a Flash EA1112HT coupled to a MAT253 mass spectrometer (Thermo Fisher Scientific, Inc.). The standard deviation based on replicate analyses was 0.02% for OC, 0.005% for TN and 0.15‰ for $\delta^{13}C$.

2.3. Lipid extraction and analysis

The procedures for lipid extraction and analysis were modified from Hopmans et al. (2000) and Sun et al. (2011). After addition of squalane and C_{46} GDGT as internal standards, the freeze-dried, homogenous sediment (10 g) was ultrasonically extracted with 20 ml dichloromethane (DCM):methanol (3:1 v:v) for 15 min (3×). The combined extracts were rotary-evaporated to near dryness and transferred to small vials. The total lipid extracts were separated into an apolar fraction by 5 ml hexane:DCM (9:1 v:v) and a polar fraction by 5 ml DCM:methanol (1:1 v:v).

The apolar fraction containing *n*-alkanes was analyzed with an Agilent 7890A gas chromatograph with flame ionization detector (GC–FID). The GC–FID was equipped with an HP5 capillary column (30 m; 0.32 mm i.d.; 0.25 μm film thickness). The injector temperature was 300 °C. A 1 μl volume of sample was injected in splitless mode under a constant flow (1.5 ml min^{-1}). Helium (purity > 99.999%) was the carrier gas. The GC oven temperature was increased from 60 to 300 °C at a rate of 6 °C min^{-1} with a final isothermal at 300 °C for 20 min. The *n*-alkanes were quantified based on peak areas by comparison with the internal standard (squalane).

The polar fraction containing GDGTs was dissolved in hexane: propanol (99:1 v:v) and filtered through a PTFE filter (0.45 μm pore size). GDGTs were analyzed on an Agilent 1200 high performance liquid chromatography-atmospheric pressure chemical ionization-Agilent 6460 mass spectrometer (HPLC–APCI–MS). The injection volume was 5 μl. The separation was achieved on a normal-phase Alltech Prevail Cyano column (150 mm × 2.1 mm; 3 μm) at a constant flow of 0.2 ml per min. The elution solvents were hexane (A) and hexane/isopropanol (9:1 v:v; B). GDGTs were eluted isocratically with 10% B for 5 min and linear gradient to 80% B in 45 min followed by a column wash with 100% B for 10 min. The APCI and MS conditions were: vaporizer pressure of 4.2×10^5 Pa, vaporizer temperature of 400 °C, drying gas flow of 6 l min^{-1}, temperature of 200 °C, capillary voltage of 3500 V, and corona current of 5 μA (3.2 kV). GDGTs were quantified based on comparisons of the respective protonated-ion peak areas of each GDGT to an internal standard (IS; C_{46} GDGT) in selected ion monitoring (SIM) mode. The protonated ions were *m/z* 1302, 1300, 1298, 1296, 1050, 1048, 1046, 1036, 1034, 1032, 1022, 1020, 1018 and 744 (IS).

2.4. Calculations of GDGT-based proxies

TEX_{86} was calculated following the equation of Schouten et al. (2002):

$$TEX_{86} = \frac{2 + 3 + 5'}{1 + 2 + 3 + 5'} \quad (1)$$

$$T = -18.6 + 66.6 \times TEX_{86}. \quad (2)$$

An updated TEX_{86}–SST (sea surface temperature) calibration equation from Kim et al. (2010) was also used in order to compare the reconstructed temperature from different calibration equations.

$$TEX_{86}^{L} = \frac{1}{1 + 2 + 3} \quad (3)$$

$$SST = 67.5 \times TEX_{86}^{L} + 46.9. \quad (4)$$

The BIT index is defined as the abundance ratio of branched GDGT-I, II and III to crenarchaeol (Hopmans et al., 2004).

$$BIT = \frac{I + II + III}{I + II + III + 5}. \quad (5)$$

The MBT and CBT proxies were first proposed by Weijers et al. (2007a), but the derived soil pH and mean air temperature (MAT) were calculated according to the revised calibration (MBT′/CBT) of Peterse et al. (2012).

$$MBT = \frac{I + Ib + Ic}{I + Ib + Ic + II + IIb + IIc + III} \quad (6)$$

$$CBT = -\log\left(\frac{Ib + IIB}{I + II}\right) \quad (7)$$

$$pH = 7.90 - 1.97 \times CBT \quad (8)$$

$$MAT = 0.81 - 5.67 \times CBT + 31.0 \times MBT. \quad (9)$$

The numbers in the above equations refer to the GDGTs drawn in Fig. 1, where I, II and III are *b*GDGTs, and 5 and 5′ are crenarchaeol and its regioisomer, respectively.

2.5. Statistical analysis

All reported correlation coefficients (r) are based on linear ordinary least squares regressions computed using the Microsoft Excel (Version 2007 for Windows), and p-values were calculated based on one-way analysis of variance (ANOVA). In addition, a principal component analysis (PCA) was performed based on the concentration of GDGTs and long-chain *n*-alkanes to identify the relationships among biomarkers. The ANOVA and PCA were performed using the SPSS 16.0 program (SPSS Inc., Chicago, Illinois).

3. Results

3.1. Bulk organic matter properties

Organic carbon (OC) in sediments ranged from 0.02% to 0.34% with an average of 0.13% (Fig. 3a). No significant difference ($p > 0.05$) was observed for sedimentary OC content from the river to the coast. The nitrogen (N) content was lower than 0.033% (data not shown), displaying a similar distribution pattern to OC. The OC/N ranged from 9.5 to 36.0 (avg. 21.9) in the lower YR, 8.6 to 12.4 (avg. 10.6) in the modern estuary, 8.5 to 28.0 (avg. 15.2) in the old estuary, and 11.2 to 28.0 (avg. 18.3) at the coast (Fig. 3), presenting significant differences from the river to the sea ($p < 0.05$). The $\delta^{13}C$ values fell in a range of −24.2‰ to −21.9‰, exhibiting an increasing trend seaward (Fig. 3c). The C3 land plants and marine plankton have an average $\delta^{13}C$ value of approximately −27‰ and −20‰, respectively (Meyers, 1997). Hence, the $\delta^{13}C$ distribution pattern in the YR-dominated margin reflected a gradual seaward decrease in the relative contribution of terrestrial organic matter to the sedimentary organic carbon pool. The median grain size of sediments changed from 6.3 to 87.5 μm (Fig. 3d). A negative correlation between the OC content and the median grain size ($r = -0.89$) suggests that sedimentary organic matter was mainly associated with fine particles.

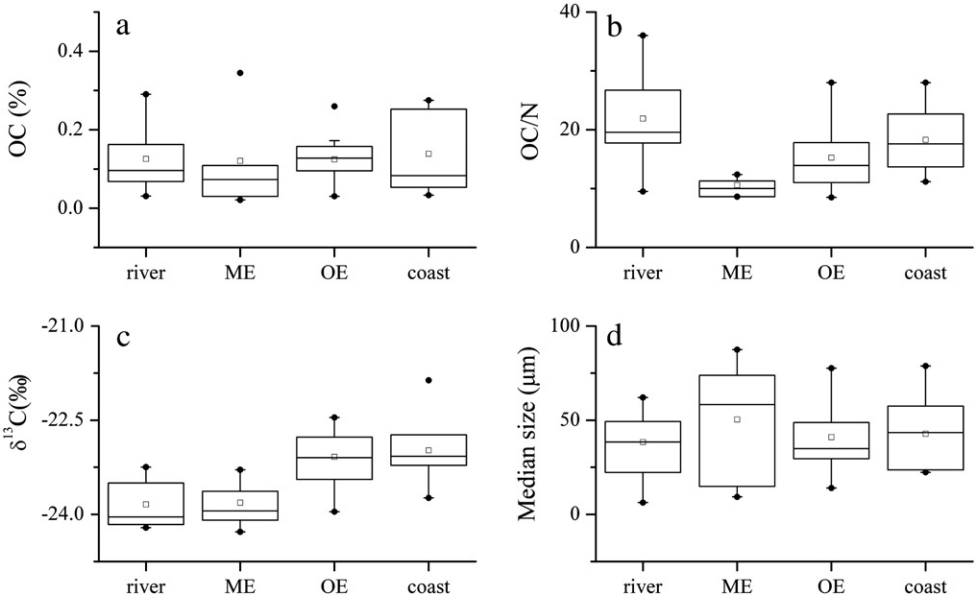

Fig. 3. Box plots showing distributions of bulk parameters in surface sediments along the transect of the lower Yellow River (river), modern estuary (ME), old estuary (OE) to the coast. The box plots parameters from bottom to top presenting the lower extreme, lower quartile, median, average, upper quartile and upper extreme values, respectively. a) OC (%); b) C/N; c) $\delta^{13}C$ (‰); and d) median grain size (μm).

3.2. GDGTs in soils and sediments

The *b*GDGTs and *i*GDGTs were detected in all CLP soils with an average concentration of 5.33 ± 7.46 μg g^{-1} OC (mean ± SD; same hereafter) (Table 1). The *b*GDGTs and crenarchaeol accounted for 51.2% ± 19.1% and 25.0% ± 10.8% of total GDGTs, respectively. The BIT index had an average value of 0.61 ± 0.18, and the GDGT-0/crenarchaeol was 0.60 ± 0.43.

For sediments, the total GDGT concentrations varied from 10.9 to 66.6 μg g^{-1} OC. The relative abundance of bacterial *b*GDGTs gradually decreased from the lower YR to the coast, accounting for 70 ± 11% of total GDGTs in the lower YR, 74 ± 8.1% in the modern estuary, 56 ± 9.8% in the old estuary and 35 ± 14% at the coast (Table 1). The concentration of *i*GDGTs consistently increased toward the sea (7.2 μg g^{-1} OC in the lower YR vs. 23.4 μg g^{-1} OC at the coast; Fig. 4), while the average concentration of *b*GDGTs, which ranged from 11.6 to 26.3 μg g^{-1} OC, did not show a clear spatial trend (Fig. 4). The BIT index in the lower YR (0.81 ± 0.10) and the modern estuary (0.79 ± 0.10) was substantially higher than that in the old estuary (0.59 ± 0.12) and at the coast (0.36 ± 0.14), reflecting a deceasing contribution of terrestrial organic matter toward the sea (Fig. 4). The weighed ratio of GDGT-0/crenarchaeol gradually decreased from the river to the coast with an average of 1.62 ± 0.59 in the lower YR, 1.06 ± 0.23 in the modern estuary, 0.82 ± 0.27 in the old estuary and 0.60 ± 0.14 at the coast (Table 1).

3.3. GDGT-based temperature proxies

The CBT index (−0.15 to 0.28) did not show a clear spatial trend from the lower YR to the coast (Table S1). In contrast, the MBT index displayed a slightly increasing trend toward the sea, ranging from 0.25 to 0.35 (avg. 0.29) in the YR, 0.28 to 0.32 (avg. 0.30) in the modern estuary, 0.28 to 0.40 (avg. 0.35, except site C2) in the old estuary and 0.34 to 0.39 (avg. 0.37) at the coast (Table S1). Based on the global MBT′/CBT calibration equations (Peterse et al., 2012), the reconstructed pH and MAT for our whole study area fell in the range of 7.3 to 8.2 (avg. 7.7; Fig. 5a) and 7.6 to 12.8 °C (avg. 10.2 °C; Fig. 5b), respectively. Meanwhile, the TEX_{86} index varied from 0.47 to 0.71, corresponding to a temperature range of 12.7 to 28.4 °C. The TEX_{86}-derived temperature was much higher in the lower YR (24.4 ± 3.1 °C) and the modern estuary (21.7 ± 3.9 °C) than in the old estuary (18.3 ± 3.4 °C) and at the coast (14.2 ± 1.3 °C) (Fig. 5c).

Table 1
Data summary on GDGTs (μg g^{-1} OC) and LCA (μg g^{-1} OC) in surface sediments along the transect of lower Yellow River (River), modern estuary (ME), old estuary (OE) and the coast.

Area	Site	Total GDGTs	*b*GDGT	*i*GDGT	Cren[a]	GDGT-0	LCA[b]	*b*GDGT (%)	GDGT-0/cren	BIT
CLP[c]	Mean	5.33	2.88	2.45	1.23	0.74	–	51	0.60	0.61
River	A1	12.9	10.2	2.71	0.80	1.4	0.16	79	1.75	0.88
	A2	32.6	23.5	9.12	3.85	3.46	0.24	72	0.9	0.79
	A3	15.4	8.51	6.86	1.80	4.1	0.79	55	2.28	0.76
	A4	34.2	27.8	6.4	2.03	3.09	0.13	81	1.52	0.89
	A5	34.4	15.4	19	8.22	7.1	0.44	45	0.86	0.53
	A6	10.9	8.44	2.43	0.73	1.33	0.35	78	1.84	0.88
	A7	11.9	7.75	4.18	1.35	2.08	0.28	65	1.54	0.78
	A8	20.2	12.4	7.88	2.29	4.39	0.57	61	1.92	0.78
	A9	15.8	12.1	3.62	0.93	2.06	0.14	77	2.22	0.88
	A10	66.6	53.0	13.6	5.73	5.07	0.48	80	0.88	0.85
	A11	24.5	19.1	5.36	1.27	3.33	0.29	78	2.62	0.91
	A12	14.4	9.64	4.78	1.71	1.99	0.27	67	1.16	0.75
ME	B1	54.5	43.0	11.5	4.34	5.06	0.66	79	1.16	0.86
	B2	23.7	18.0	5.71	2.26	2.35	0.2	76	1.04	0.82
	B3	33.5	23.3	10.2	4.38	4.31	0.23	70	0.99	0.76
	B4	33.4	27.5	5.86	1.97	2.25	0.13	82	1.14	0.87
	B5	29.1	24.3	4.86	1.79	2.37	0.42	83	1.32	0.89
	B6	45.2	31.7	13.5	4.82	6.23	0.20	70	1.29	0.74
	B7	39.4	23.1	16.4	9	5.34	0.16	59	0.59	0.6
	B8	26.6	19.5	7.11	3.01	2.85	0.11	73	0.95	0.76
OE	C1	31.6	15.3	16.4	8.75	5.42	0.28	48	0.62	0.52
	C2	16.7	7.14	9.59	5.13	3.32	0.27	43	0.65	0.46
	C3	45.6	20.0	25.6	13.2	8.86	0.29	44	0.67	0.48
	C4	33.6	16.6	17.1	8.83	5.87	0.28	49	0.66	0.53
	C5	28.4	13.7	14.7	7.64	4.99	0.19	48	0.65	0.52
	C6	16.3	8.11	8.21	4.09	2.95	0.11	50	0.72	0.53
	C7	39.8	22.4	17.4	8.73	6.22	0.22	56	0.71	0.53
	C8	37.4	23.7	13.7	6.5	5.32	0.35	63	0.82	0.69
	C9	13.7	9.56	4.12	1.47	2.14	0.32	70	1.46	0.81
	C10	20.9	10.5	10.3	5.05	3.59	0.13	50	0.71	0.49
	C11	16.9	10.9	5.98	2.18	3.01	0.18	65	1.38	0.75
	C12	32.2	23.1	9.04	4.09	3.25	0.10	72	0.79	0.7
	C13	24.3	14.9	9.48	4.34	3.70	0.24	61	0.85	0.68
Coast	D1	41.9	19.5	22.3	11.4	7.75	0.22	47	0.68	0.5
	D2	48.4	10.2	38.2	23.9	9.45	0.38	21	0.39	0.2
	D3	43.3	9.83	33.5	20.2	8.97	0.36	23	0.44	0.22
	D4	35.3	6.92	28.4	16.7	8.57	0.35	20	0.51	0.21
	D5	22.1	9.23	12.8	6.76	4.69	0.21	42	0.69	0.44
	D6	27.6	11.7	15.9	8.2	5.66	0.18	42	0.69	0.43
	D7	25.8	13.4	12.4	6.02	4.62	0.10	52	0.77	0.51

Data from Yang (unpublished data).
[a] Cren: crenarchaeol.
[b] LCA: long chain *n*-alkanes (C_{27} + C_{29} + C_{31} *n*-alkanes).
[c] CLP: Chinese loess plateau.

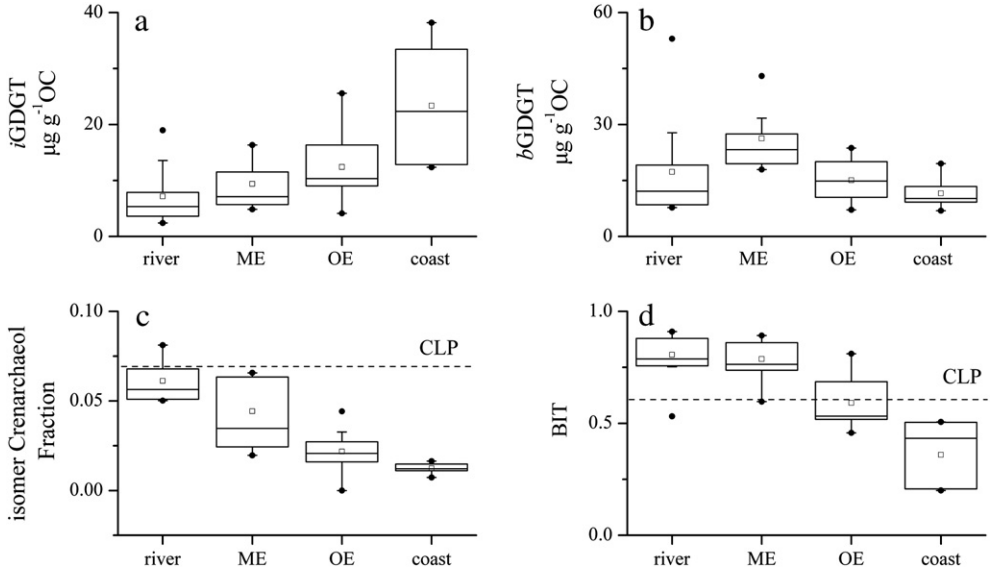

Fig. 4. Box distributions of GDGTs in the surface sediments along the transect of the lower Yellow River (river), modern estuary (ME), old estuary (OE) and the coast. The box plots parameters from bottom to top presenting the lower extreme, lower quartile, median, average, upper quartile and upper extreme values, respectively. a) *i*GDGT (μg g^{-1} OC); b) *b*GDGT (μg g^{-1} OC); c) isomer crenarchaeol fraction; and d) BIT.

4. Discussion

4.1. Distribution and source of GDGTs from river to coast

Although thought to be mainly biosynthesized by pelagic Thaumarchaeota, *i*GDGTs are detected in almost all soil and peat samples of the world (Weijers et al., 2006a). This terrestrial-derived *i*GDGT can be transported to aquatic systems via runoff, making *i*GDGT (e.g., crenarchaeol) not solely of in situ production. In our study, crenarchaeol was ubiquitous in the CLP soils with an average concentration of 1.23 ± 1.39 μg g^{-1} OC (Table S1). The relative abundance of crenarchaeol in the CLP soils (25.0% of total GDGTs) was substantially higher than the global average (ca. 9% based on 58 samples from 26 globally-distributed locations; Weijers et al., 2006a). Higher relative abundances of crenarchaeol have been in soils of higher pH (Weijers et al., 2006a). Thus, the abundance of *i*GDGT in the CLP is no surprise since its alkaline soils (avg. pH 7.9) provide favorable living conditions for Thaumarchaeota (Xie et al., 2012; Yang et al., 2012).

In order to identify the sources of *i*GDGT in the YR-dominated continental margin, we calculated the ratio of crenarchaeol regioisomer:(crenarchaeol + crenarchaeol regioisomer). Sinninghe Damsté et al. (2012) found that the soil and marine Thaumarchaeota could biosynthesize crenarchaeol and its regioisomer in relative abundances of 10%–20% and <5%, respectively. The crenarchaeol regioisomer / (crenarchaeol + crenarchaeol regioisomer) was 6.1 ± 1.1% in the lower YR sediments, very close to that in surface CLP soils (6.9 ± 3.1%) (Fig. 4). The relative abundance of the crenarchaeol regioisomer decreased from lower YR to the sea with an average of 4.4 ± 2.0% in the modern estuary, 2.2 ± 1.1% in the old estuary and 1.2 ± 1.3% at the coast (Fig. 4), reflecting increasing contributions of marine Thaumarchaeota. Along this transect, the crenarchaeol concentration steadily increased from 2.6 ± 2.3 μg g^{-1} OC in the lower YR,

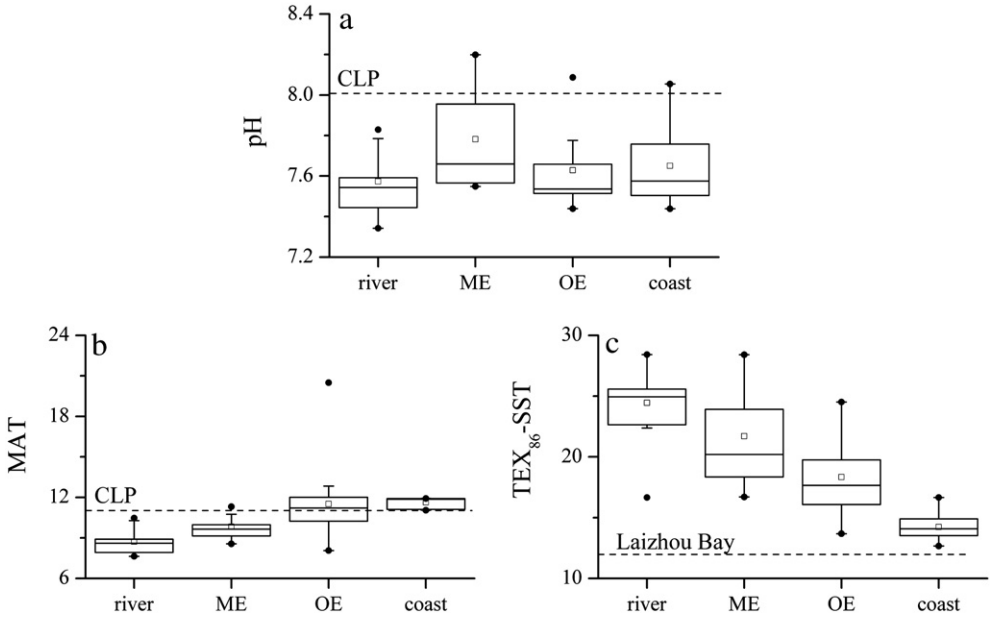

Fig. 5. GDGT-reconstructed pH (a), annual mean air temperature (MAT; b) and sea surface temperature (SST; c) in the Yellow River dominated continental margin.

4.0 ± 2.4 μg g^{-1} OC in the modern estuary, 6.2 ± 3.2 μg g^{-1} OC in the old estuary and 13.3 ± 7.0 μg g^{-1} OC at the coast (Table 1). Since methanogenic archaea and Thaumarchaeota have a GDGT-0 to crenarchaeol ratio of >2.0 and 0.2–2.0, respectively (Blaga et al., 2009; Sinninghe Damsté et al., 2009), the continuous decrease in this ratio from the lower YR (avg. 1.62) to the coast (avg. 0.60) suggests a greater contribution of aquatic Thaumarchaeota to *i*GDGTs toward the sea (Fig. 4). The GDGT distribution pattern strongly supports that *i*GDGTs in the lower YR were primarily derived from erosion of the CLP soil, but those found in the estuarine and coastal areas were of mixed inputs from in situ production and fluvial terrestrial inputs.

The *b*GDGTs are mainly produced by unknown bacteria thriving in soil and peat (Hopmans et al., 2004; Weijers et al., 2006b). Consequently, the presence of *b*GDGTs in aquatic environments is often indicative of an allochthonous terrestrial input. Nevertheless, recent studies have demonstrated in situ biosynthesis of *b*GDGTs in lakes (Bechtel et al., 2010; Tierney and Russell, 2009; Wang et al., 2012) and rivers (Kim et al., 2012; Zell et al., 2013; Zhu et al., 2011). Unlike *i*GDGTs, the abundance of *b*GDGTs did not show a clear trend from the YR to the coast (Fig. 4). Our statistical analyses revealed no significant difference in *b*GDGTs between the lower YR, the old estuary and the coast ($p > 0.05$), but the modern estuary had significantly higher concentrations of *b*GDGT (avg. 26.3 μg g^{-1} OC) than the other sites ($p < 0.05$). The reason for the abundance of *b*GDGTs in the modern estuary remains elusive, probably due to preferential preservation of soil-derived *b*GDGTs in the highly dynamic YR estuary. This is corroborated by Huguet et al. (2008) who observed that soil-derived *b*GDGTs were better preserved (7–20%) than marine-derived crenarchaeol (0.2–3%) under long-term oxygen exposure. Because over 90% of YR sediments originate from soil erosion in the CLP (Ren and Shi, 1986), we attributed *b*GDGTs in the YR-dominated continental margin to a terrestrial origin. This conclusion is supported by similar distributions of *b*GDGTs I, II and III among the CLP, YR, estuarine and coastal sediments (Fig. 6).

A detailed analysis of the BIT index showed an increasing trend offshore in the old estuary (from 0.46 to 0.81) and the coast (from 0.2 to 0.51 except D1) (Fig. 7). This result is unexpected because the BIT index, an indicator for soil organic matter (Hopmans et al., 2004), usually decreases with increasing distance from the shoreline (Herfort et al., 2006; Hopmans et al., 2004). Our observed BIT distribution is, however, consistent with the sediment dispersal pattern of the present YR subdelta where the wave-induced alongshore current and shear front greatly influence fluvial sediment transport (Fig. 2) (Bi et al., 2010). Under the joint effect of these two currents, the fluvial sediments

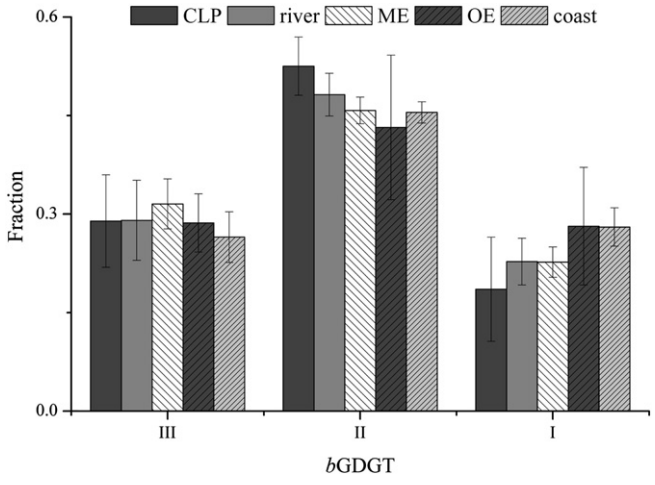

Fig. 6. Relative abundance of branched GDGTs I, II and III in surface soils of the Chinese loess plateau (CLP) and surface sediments of the lower Yellow River (river), modern estuary (ME), old estuary (OE) and the coast.

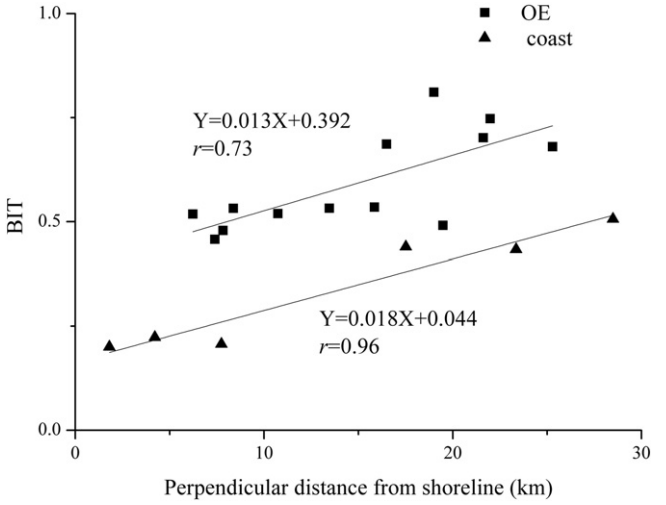

Fig. 7. Variability of the BIT values with the perpendicular distance from the shoreline in the old estuary (square) and the coast (triangle), Bohai Sea.

of the YR are primarily deposited in offshore areas within the 5 m isobath rather than in nearshore areas. In other words, more fluvial-derived terrestrial organic matter is buried offshore, resulting in higher BIT values there.

4.2. Proportion and transport of terrestrial organic matter in the YR-dominated continental margin

Large river-dominated continental margins are characterized by complex organic matter sources including autochthonous marine and allochthonous terrestrial organic matter derived from rivers and coastal erosion. Stable carbon isotopic signatures ($\delta^{13}C$), the organic carbon to nitrogen ratio (OC/N) and biomarkers (e.g., BIT) have been used to estimate the relative contribution of terrestrial organic matter to the sedimentary organic carbon pool (Meyers, 1997; Zhu et al., 2011; Wu et al., 2013). Since each proxy has intrinsic drawbacks, a multi-proxy approach was recommended (Herfort et al., 2006; Meyers, 1997). Here, we used a binary mixing model to estimate the relative amount of terrestrial organic carbon based on $\delta^{13}C$, OC/N and BIT, expressed as:

$$X_{sed} = f_{terr}X_{terr} + f_{aqu}X_{aqu}$$

$$f_{terr} + f_{aqu} = 1$$

where f_{terr} and f_{aqu} refer to the terrestrial and aquatic OC fractions, respectively; X_{terr} and X_{aqu} are the terrestrial and aquatic end-member values of the respective proxies; and X_{sed} refers to the proxy analyzed.

Based on this study, the average values of $\delta^{13}C$, OC/N and BIT in the lower-YR sediments were −23.8‰, 21.9 and 0.81, respectively. These values were used as the terrestrial end-member values in our binary mixing model. Cai and Cai (1993) reported that marine organisms in the Bohai Sea had an average $\delta^{13}C$ of −20.9‰, consistent with the $\delta^{13}C$ values of typical marine organic matter (−19‰ to −21‰; Fry and Sherr, 1989). Hu et al. (2009) proposed a OC/N of 6.7 for marine organic matter in the Bohai Sea, whereas Hopmans et al. (2004) reported that marine environments had a BIT index of 0 (Hopmans et al., 2004). Hence, we used −20.9‰, 6.7 and 0 as the marine end-member values for $\delta^{13}C$, OC/N and BIT, respectively.

Since the BIT index is a ratio of *b*GDGTs to crenarchaeol, its variability is not only influenced by soil-derived *b*GDGTs, but also by marine-derived crenarchaeol (Fietz et al., 2012). Consequently, Smith et al. (2012) proposed an alternative approach to calculate the relative contribution of soil organic matter to the sedimentary organic carbon

pool (%OM_{soil}) based on the *b*GDGT abundance in soil of source regions, expressed as:

$$\%OMsoil = ([B]sample \times 100)/[B]soil$$

where $[B]_{sample}$ and $[B]_{soil}$ are the concentrations of *b*GDGTs I, II and III in sediment samples and soil, respectively. The mean concentration of *b*GDGTs I, II and III in the CLP soils (avg. 2.2 μg g^{-1} OC) was lower than in the lower-YR sediments (avg. 10.6 μg g^{-1} OC), suggesting preferential preservation of soil *b*GDGTs during long-range transport from the source region (CLP) to the lower-YR (Huguet et al., 2008, 2009). Because there was a large range of GDGT abundances in the CLP (0.05 to 49.3 μg g^{-1} OC), we used 10.6 μg g^{-1} OC as the terrestrial end-member value.

Application of binary mixing models based on the BIT index showed that terrestrial organic carbon accounted for 97 ± 12% of the sedimentary organic carbon pool in the modern estuary, 73 ± 14% in the old estuary and 44 ± 18% at the coast. Meanwhile, the $\delta^{13}C$-based calculation indicated that the average terrestrial organic carbon fraction was 100 ± 11% in the modern estuary, 75 ± 17% in the old estuary and 72 ± 20% at the coast, whereas the OC/N-based calculation yielded values of 26 ± 11% in the modern estuary, 56 ± 37% in the old estuary and 76 ± 37% at the coast (Table 2). Based on the *b*GDGT concentration, the fraction of terrestrial organic carbon was 136 ± 50% in the modern estuary, 79 ± 28% in the old estuary and 61 ± 22% at the coast (Table 2). The apparent overestimation and large standard error of the latter estimates in the modern estuary are likely caused by the large variability in the *b*GDGT abundance in the lower YR sediments (from 7.8 to 53.0 μg g^{-1} OC), resulting in a large uncertainty of the soil end-member values used in our model.

The binary mixing model based on all proxies, except OC/N, showed a consistent decrease in the relative amount of terrestrial organic carbon toward the sea. The abnormally low terrestrial organic carbon contribution in the modern estuary derived from OC/N (26%) was probably caused by interference of mineral-associated inorganic nitrogen. However, an extremely low y-intercept (0.006%) in the plot of N versus OC for the samples in the modern estuary ($r = 0.95$) suggests that the contribution of inorganic nitrogen alone is not sufficient to explain the low OC/N in the modern estuary. Alternatively, the preferential utilization of N by microbial degradation and the accumulation of microbial organic matter in sediments can lower the OC/N (Meyers, 1997). Compared to $\delta^{13}C$, the GDGT-based proxies generally gave lower terrestrial organic carbon fractions, e.g., 44% (BIT) vs. 61% (*b*GDGTs) vs. 72% ($\delta^{13}C$) at the coast. Such discrepancy could be explained by the fact that the BIT index and *b*GDGTs are of specific indicators for soil rather than bulk terrestrial organic matter (Smith et al., 2010; Walsh et al., 2008; Weijers et al., 2006b).

4.3. Applicability of MBT/CBT and TEX_{86} proxies

The MBT/CBT proxies have been applied to marine sediments of the Congo Fan (Weijers et al., 2007b), the Yangtze River shelf (Zhu et al., 2011) and high latitude environments (Peterse et al., 2009) to reconstruct continental MAT and soil pH. In our study, the CBT-derived pH ranged from 7.3 to 8.2 (avg. 7.7, Fig. 5a), close to the average pH of modern soil in the CLP (5.5–9.1, avg. 8.0) (Xu et al., 2006; Yang, unpublished data). The 0.3 pH unit difference between the average estimated and measured values is less than the calibration error of the CBT proxy (RMSE = 0.8; Peterse et al., 2012). The MBT/CBT-based MAT ranged from 7.6 to 12.8 °C with an average of 10.1 °C (Fig. 5b), consistent with the annual MAT of the middle YR basin (ca. 11 °C) (Chen et al., 2005), a major source region for the YR sediments (Ren, 2006). The minor difference (0.9 °C) between the estimated and measured averages is much less than the calibration error of the MBT′/CBT proxies (RMSE of 5.7 °C; Peterse et al., 2012). Thus, our results confirmed the validity of the MBT/CBT proxies in the YR-dominated continental margin.

The reconstructed temperature based on Eqs. (2) (Schouten et al., 2002) and (4) (Kim et al., 2010) is consistent with each other (a mean difference of 1.9 °C; Table S1). Given this, we only discuss the result from Eq. (2) hereafter. From the lower YR to the coast, the TEX_{86}-derived temperature varied from 12.7 to 28.4 °C, with a mean value of 24.4 ± 3.4 °C in the lower YR, 21.7 ± 3.9 °C in the modern estuary, 18.3 ± 3.5 °C in the old estuary and 14.2 ± 1.4 °C at the coast (Fig. 5c). The large TEX_{86}-temperature variability could be attributed to spatial changes in the source of *i*GDGTs as terrestrial and aquatic organisms may have different responses to growth temperature (see Section 4.2). With the exception of the coastal area, the reconstructed temperature was substantially higher than the annual mean temperature in the YR-dominated margin (i.e., 12 °C) (Zhang et al., 2006). Following an analysis of surface sediments from 82 lakes, Blaga et al. (2010) suggested that the TEX_{86} proxy is valid only when the GDGT-0/crenarchaeol is <2.0 and BIT is <0.4. In our dataset, all samples had a GDGT-0/crenarchaeol lower than 2.0, but only those from the coastal area had a BIT value lower than 0.4 (Table 1). So our result from the YR-dominated margin agrees well with the results of the lake study (Blaga et al., 2010).

4.4. Principal component analysis

To further understand the relationship between individual *b*GDGTs and *i*GDGTs in the YR-dominated margin, a principal component analysis (PCA) was performed. The data used in the PCA included fifteen GDGT compounds (Table 1) and long-chain *n*-alkanes (C_{27} + C_{29} + C_{31}; LCA; Table S1) from forty surface sediments in the YR-dominated margin (Fig. 1). PCA results showed that the first four principal components (PCs) accounted for 90.3% of the total variances, each of which

Table 2
Relative amounts (%) of terrestrial organic matter in surface sediments from the modern Yellow River estuary (ME), old Yellow River estuary (OE) and the nearby coast based on different proxies.

	$\delta^{13}C$	C/N	BIT	*b*GDGTs
ME	100 ± 11	26 ± 11	97 ± 12	136 ± 50
OE	75 ± 17	56 ± 37	73 ± 14	79 ± 28
Coast	72 ± 20	76 ± 37	44 ± 18	61 ± 22

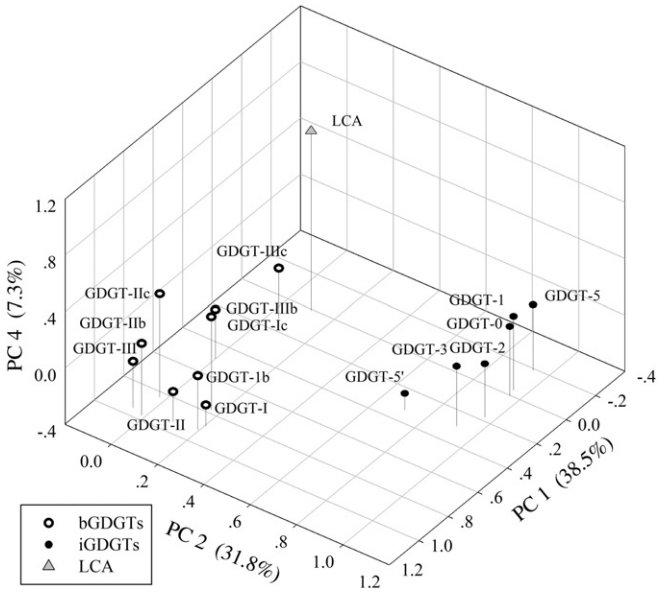

Fig. 8. The 3D plot of principal component analysis (PCA) based on 40 sediment samples from the Yellow River dominated continental margin. LCA: long chain *n*-alkanes.

accounted for 38.5%, 31.8%, 12.7% and 7.3%, respectively (Fig. 8). Based on the 3D PCA plot, all *b*GDGTs, except for *b*GDGT IIIc, had high positive loadings on PC 1 (0.49 to 0.95) and low loadings on PC 2 (−0.06 to 0.20), while all *i*GDGTs had high positive loadings on PC 2 (0.71 to 0.96) and relatively low loadings on PC 1 (−0.19 to 0.33). This result was consistent with the multiplicity of *b*GDGTs (soil origin) and *i*GDGTs (mixed soil and aquatic origin) in the YR-dominated margin (see Section 4.1). Unexpectedly, LCA was clearly separated from *b*GDGTs in the PCA plot (Fig. 8) although both are proxies of terrestrial organic matter (Meyers, 1997; Hopmans et al., 2004). In the PCA plot, LCA had extremely low loadings on PC 1 (0.007) and PC 2 (0.10), but high positive loading on PC 4 (0.88). The low correlation between LCA and *b*GDGTs ($r < 0.15$; $p > 0.2$) was likely due to different transport pathways, which resulted in different distribution patterns. Soil-associated *b*GDGTs are exclusively supplied by runoff, whereas plant-derived LCA can be subjected to both atmospheric transport and riverine transport (Hopmans et al., 2004; Walsh et al., 2008). In the YR-dominated margin, atmospheric transport is particularly important in the winter when the strong northwestern winds from land to ocean predominate during the East Asian Winter Monsoon (Fu et al., 2002).

4.5. Implications of GDGT-proxies in river-dominated margins

The world's 10 largest rivers, including the YR, transport approximately 40% of the fresh water and particulate matter to the sea (Milliman and Meade, 1983). Consequently, coastal areas under the influence of these large rivers are characterized by high primary productivity and high sedimentation rates. Despite its importance on the global carbon cycling and environmental changes, the source and chemical composition of sedimentary organic carbon in the river-dominated margins display highly spatial and temporal heterogeneity, and its biogeochemical behavior is not well understood (Bianchi et al., 2002). Among the commonly used source indicators such as $\delta^{13}C$, C/N, long-chain *n*-alkanes and lignin, each has intrinsic drawbacks (Herfort et al., 2006). Thus, the GDGT-based proxies (the BIT index, MBT/CBT and TEX_{86}) provide additional tracers to evaluate organic carbon source and sea/continental temperature. It was originally assumed that, in aquatic environments, *i*GDGTs are mainly derived from aquatic Thaumarchaeota, whereas *b*GDGTs are allochthonous and derived from soil bacteria (Hopmans et al., 2004; Schouten et al., 2002; Weijers et al., 2006a, 2007a). However, based on the study of globally-distributed sites, Fietz et al. (2012) found a significant correlation between the concentrations of *b*GDGTs and crenarchaeol ($p < 0.01$; $r^2 = 0.57–0.99$), indicating that a common or mixed source for both GDGT types is typical in lacustrine and marine settings. Given the ongoing debate on GDGT sources, more studies are needed. Our work in the YR-dominated margin supports different origins for *b*GDGTs and *i*GDGTs. The constant and predominant soil origin of *b*GDGTs confirms the reliability of the MBT/CBT proxies to record continental temperature and pH of the CLP, whereas the variability/multiplicity of the *i*GDGTs' sources from the YR to the coast causes significant deviation of the TEX_{86}-derived temperature from actual values. Thus, our study highlights that the provenance of GDGTs is an important factor in determining the accuracy of the GDGT-based proxies, which should be kept in mind when these proxies are applied to other environments where terrestrial inputs are significant.

5. Conclusions

We conducted a comprehensive study on the composition and distribution of GDGTs in surface sediments of the YR-dominated continental margin. The distribution pattern of GDGTs and the PCA demonstrated that *b*GDGTs were strictly derived from soil erosion of the Chinese loess plateau, whereas *i*GDGTs varied in source by location, they were primarily derived from soil erosion in the lower YR and modern estuary, but originated from both soil and in situ production in the old estuary and the coastal area. Consequently, the *b*GDGT-based MBT/CBT proxies reliably recorded the temperature and pH signals of the CLP, while the *i*GDGT-based TEX_{86} proxy returned large deviations from the actual temperature. Our study highlights that the provenance of GDGTs must be determined before they can be used confidently as environmental indicators. The assessment of the terrestrial organic matter contribution to the sedimentary organic carbon pool in the estuarine/coastal areas, based on the BIT, $\delta^{13}C$ and *b*GDGT concentrations, was generally consistent with each other, demonstrating the applicability of these proxies in the YR-dominated margin. Nevertheless, in agreement with previous studies (e.g., Walsh et al., 2008; Smith et al., 2012), estimates of the terrestrial organic matter fraction, based on the GDGT-proxies, were lower than those from the $\delta^{13}C$, and were attributed to the fact that *b*GDGTs are specific to soil organic matter, whereas the $\delta^{13}C$ is related to bulk organic carbon content.

Supplementary data to this article can be found online at http://dx.doi.org/10.1016/j.marchem.2013.11.006.

Acknowledgments

This study was financially supported by NSFC (41006042, 41176164) and the Ministry of Education, China (SRFDP). We thank Leilei Zhang for assistance in sample analyses. We are grateful to Richard Smith, Alfonso Mucci and two anonymous reviewers for their constructive comments.

References

Bechtel, A., Smittenberg, R.H., Bernasconi, S.M., Schubert, C.J., 2010. Distribution of branched and isoprenoid tetraether lipids in an oligotrophic and a eutrophic Swiss lake: insights into sources and GDGT-based proxies. Org. Geochem. 41, 822–832. http://dx.doi.org/10.1016/j.orggeochem.2010.04.022.

Bi, N., Yang, Z., Wang, H., Hu, B., Ji, Y., 2010. Sediment dispersion pattern off the present Huanghe (Yellow River) subdelta and its dynamic mechanism during normal river discharge period. Estuar. Coast. Shelf Sci. 86, 352–362. http://dx.doi.org/10.1016/j.ecss.2009.06.005.

Bianchi, T.S., Mitra, S., McKee, B.A., 2002. Sources of terrestrially-derived organic carbon in lower Mississippi River and Louisiana shelf sediments: implications for differential sedimentation and transport at the coastal margin. Mar. Chem. 77, 211–223. http://dx.doi.org/10.1016/S0304-4203(01)00088-3.

Blaga, C., Reichart, G., Heiri, O., Sinninghe Damsté, J., 2009. Tetraether membrane lipid distributions in water-column particulate matter and sediments: a study of 47 European lakes along a north–south transect. J. Paleolimnol. 41, 523–540. http://dx.doi.org/10.1007/s10933-008-9242-2.

Blaga, C., Reichart, G., Schouten, S., Lotter, A., Werne, J., Kosten, S., et al., 2010. Branched glycerol dialkyl glycerol tetraethers in lake sediments: can they be used as temperature and pH proxies? Org. Geochem. 41, 1225–1234. http://dx.doi.org/10.1016/j.orggeochem.2010.07.002.

Cai, D., Cai, A., 1993. Isotopic geochemistry investigation of organic carbon in Yellow River estuary. Sci. China B Chem. 23, 1105–1113 (in Chinese).

Chen, J., Wang, F., Meybeck, M., He, D., Xia, X., Zhang, L., 2005. Spatial and temporal analysis of water chemistry records (1958–2000) in the Huanghe (Yellow River) basin. Glob. Biogeochem. Cycle 19, GB3016. http://dx.doi.org/10.1029/2004GB002325.

Fietz, S., Huguet, C., Bendle, J., Escala, M., Gallacher, C., Herfort, L., et al., 2012. Co-variation of crenarchaeol and branched GDGTs in globally-distributed marine and freshwater sedimentary archives. Glob. Planet. Change 92–93, 275–285. http://dx.doi.org/10.1016/j.gloplacha.2012.05.020.

Fry, B., Sherr, E.B., 1989. $\delta^{13}C$ measurements as indicators of carbon flow in marine and freshwater ecosystems. In: Rundel, P.W., Ehleringer, J.R., Nagy, K.A. (Eds.), Stable Isotopes in Ecological Research. Springer, New York, pp. 196–229.

Fu, C., Harasawa, H., Kasyanov, V., Kim, J.-W., Ojima, D., Wan, Z., Zhao, S., 2002. Regional–global interactions in East Asia. In: Tyson, P., Fu, C., Fuchs, R., Lebel, L., Mitra, A.P., Odada, E., Perry, J., Steffen, W., Virji, H. (Eds.), Global–Regional Linkages in the Earth System. Springer Berlin Heidelberg, pp. 109–149.

Herfort, L., Schouten, S., Boon, J.P., Woltering, M., Baas, M., Weijers, J.W.H., et al., 2006. Characterization of transport and deposition of terrestrial organic matter in the southern North Sea using the BIT index. Limnol. Oceanogr. 51, 2196–2205. http://dx.doi.org/10.4319/lo.2006.51.5.2196.

Hopmans, E.C., Schouten, S., Pancost, R.D., van der Meer, M.T.J., Sinninghe Damsté, J.S., 2000. Analysis of intact tetraether lipids in archaeal cell material and sediments by high performance liquid chromatography/atmospheric pressure chemical ionization mass spectrometry. Rapid Commun. Mass Spectrom. 14, 585–589. http://dx.doi.org/10.1002/(sici)1097-0231(20000415)14:7<585::aid-rcm913>3.0.co;2-n.

Hopmans, E.C., Weijers, J.W.H., Schefuß, E., Herfort, L., Sinninghe Damsté, J.S., Schouten, S., 2004. A novel proxy for terrestrial organic matter in sediments based on branched and isoprenoid tetraether lipids. Earth Planet. Sci. Lett. 224, 107–116. http://dx.doi.org/10.1016/j.epsl.2004.05.012.

Hu, L., Guo, Z., Feng, J., Yang, Z., Fang, M., 2009. Distributions and sources of bulk organic matter and aliphatic hydrocarbons in surface sediments of the Bohai Sea, China. Mar. Chem. 113, 197–211. http://dx.doi.org/10.1016/j.marchem.2009.02.001.

Huguet, C., de Lange, G.J., Gustafsson, Ö., Middelburg, J.J., Sinninghe Damsté, J.S., Schouten, S., 2008. Selective preservation of soil organic matter in oxidized marine sediments (Madeira Abyssal Plain). Geochim. Cosmochim. Acta 72, 6061–6068. http://dx.doi.org/10.1016/j.gca.2008.09.021.

Huguet, C., Kim, J.-H., de Lange, G.J., Sinninghe Damsté, J.S., Schouten, S., 2009. Effects of long term oxic degradation on the TEX_{86} and BIT organic proxies. Org. Geochem. 40, 1188–1194. http://dx.doi.org/10.1016/j.orggeochem.2009.09.003.

IRTCES, 2004. International Research and Training Center on Erosion and Sedimentation. Bulletin of Chinese River Sediment (2003).Ministry of Water Resources Conservancy, Beijing, China ((in Chinese), data available on http://www.irtces.org/database.asp).

Kim, J.-H., Schouten, S., Hopmans, E.C., Donner, B., Sinninghe Damsté, J.S., 2008. Global sediment core-top calibration of the TEX_{86} paleothermometer in the ocean. Geochim. Cosmochim. Acta 72, 1154–1173. http://dx.doi.org/10.1016/j.gca.2007.12.010.

Kim, J.-H., van der Meer, J., Schouten, S., Helmke, P., Willmott, V., Sangiorgi, F., Koç, N., Hopmans, E.C., Damsté, J.S.S., 2010. New indices and calibrations derived from the distribution of crenarchaeal isoprenoid tetraether lipids: implications for past sea surface temperature reconstructions. Geochim. Cosmochim. Acta 74, 4639–4654. http://dx.doi.org/10.1016/j.gca.2010.05.027.

Kim, J.-H., Zell, C., Moreira-Turcq, P., Pérez, M.A.P., Abril, G., Mortillaro, J.-M., et al., 2012. Tracing soil organic carbon in the lower Amazon River and its tributaries using GDGT distributions and bulk organic matter properties. Geochim. Cosmochim. Acta 90, 163–180. http://dx.doi.org/10.1016/j.gca.2012.05.014.

Li, G., Tang, Z., Yue, S., Zhuang, K., Wei, H., 2001. Sedimentation in the shear front off the Yellow River mouth. Cont. Shelf Res. 21, 607–625. http://dx.doi.org/10.1016/S0278-4343(00)00097-2.

Meyers, P.A., 1997. Organic geochemical proxies of paleoceanographic, paleolimnologic, and paleoclimatic processes. Org. Geochem. 27, 213–250. http://dx.doi.org/10.1016/S0146-6380(97)00049-1.

Milliman, J.D., Meade, R.H., 1983. World-wide delivery of river sediment to the oceans. J. Geol. 91, 1–21. http://dx.doi.org/10.2307/30060512.

Milliman, J.D., Qin, Y., Ren, M., Saito, Y., 1987. Man's influence on the erosion and transport of sediment by Asian rivers: the Yellow River (Huanghe) example. J. Geol. 95, 751–762. http://dx.doi.org/10.2307/30063822.

Pancost, R.D., Boot, C.S., 2004. The palaeoclimatic utility of terrestrial biomarkers in marine sediments. Mar. Chem. 92, 239–261. http://dx.doi.org/10.1016/j.marchem.2004.06.029.

Pang, J., Si, S., 1979. The estuary changes of Huanghe River I. Changes in modern time. Oceanol. Limnol. Sin. 19, 136–141 (in Chinese).

Peterse, F., Kim, J.-H., Schouten, S., Kristensen, D.K., Koç, N., Sinninghe Damsté, J.S., 2009. Constraints on the application of the MBT/CBT palaeothermometer at high latitude environments (Svalbard, Norway). Org. Geochem. 40, 692–699. http://dx.doi.org/10.1016/j.orggeochem.2009.03.004.

Peterse, F., van der Meer, J., Schouten, S., Weijers, J.W.H., Fierer, N., Jackson, R.B., et al., 2012. Revised calibration of the MBT–CBT paleotemperature proxy based on branched tetraether membrane lipids in surface soils. Geochim. Cosmochim. Acta 96, 215–229. http://dx.doi.org/10.1016/j.gca.2012.08.011.

Powers, L., Werne, J.P., Vanderwoude, A.J., Sinninghe Damsté, J.S., Hopmans, E.C., Schouten, S., 2010. Applicability and calibration of the TEX_{86} paleothermometer in lakes. Org. Geochem. 41, 404–413. http://dx.doi.org/10.1016/j.orggeochem.2009.11.009.

Ren, M., 2006. Sediment discharge of the Yellow River, China: past, present and future—a synthesis. Adv. Earth Sci. 6, 551–563 (in Chinese).

Ren, M., Shi, Y., 1986. Sediment discharge of the Yellow River (China) and its effect on the sedimentation of the Bohai and the Yellow Sea. Cont. Shelf Res. 6, 785–810. http://dx.doi.org/10.1016/0278-4343(86)90037-3.

Schouten, S., Hopmans, E.C., Schefuß, E., Sinninghe Damsté, J.S., 2002. Distributional variations in marine crenarchaeotal membrane lipids: a new tool for reconstructing ancient sea water temperatures? Earth Planet. Sci. Lett. 204, 265–274. http://dx.doi.org/10.1016/S0012-821X(02)00979-2.

Schouten, S., Hopmans, E.C., Sinninghe Damsté, J.S., 2013. The organic geochemistry of glycerol dialkyl glycerol tetraether lipids: a review. Org. Geochem. 54, 19–61. http://dx.doi.org/10.1016/j.orggeochem.2012.09.006.

Sinninghe Damsté, J.S., Schouten, S., Hopmans, E.C., van Duin, A.C.T., Geenevasen, J.A.J., 2002. Crenarchaeol: the characteristic core glycerol dibiphytanyl glycerol tetraether membrane lipid of cosmopolitan pelagic crenarchaeota. J. Lipid Res. 43, 1641–1651. http://dx.doi.org/10.1194/jlr.M200148-JLR200.

Sinninghe Damsté, J.S., Ossebaar, J., Abbas, B., Schouten, S., Verschuren, D., 2009. Fluxes and distribution of tetraether lipids in an equatorial African lake: constraints on the application of the TEX_{86} palaeothermometer and BIT index in lacustrine settings. Geochim. Cosmochim. Acta 73, 4232–4249. http://dx.doi.org/10.1016/j.gca.2009.04.022.

Sinninghe Damsté, J.S., Rijpstra, W.I., Hopmans, E.C., Weijers, J.W., Foesel, B.U., Overmann, J., et al., 2011. 13,16-Dimethyl octacosanedioic acid (iso-diabolic acid), a common membrane-spanning lipid of acidobacteria subdivisions 1 and 3. Appl. Environ. Microbiol. 77, 4147–4154. http://dx.doi.org/10.1128/AEM.00466-11.

Sinninghe Damsté, J.S., Rijpstra, W.I.C., Hopmans, E.C., Jung, M.Y., Kim, J.G., Rhee, S.K., et al., 2012. Intact polar and core glycerol dibiphytanyl glycerol tetraether lipids of group I.1a and I.1b Thaumarchaeota in soil. Appl. Environ. Microbiol. 78, 6866–6874. http://dx.doi.org/10.1128/aem.01681-12.

Smith, R.W., Bianchi, T.S., Savage, C., 2010. Comparison of lignin phenols and branched/isoprenoid tetraethers (BIT index) as indices of terrestrial organic matter in Doubtful Sound, Fiordland, New Zealand. Org. Geochem. 41, 281–290. http://dx.doi.org/10.1016/j.orggeochem.2009.10.009.

Smith, R.W., Bianchi, T.S., Li, X., 2012. A re-evaluation of the use of branched GDGTs as terrestrial biomarkers: implications for the BIT Index. Geochim. Cosmochim. Acta 80, 14–29. http://dx.doi.org/10.1016/j.gca.2011.11.025.

Sun, D., Tan, W., Pei, Y., Zhou, L., Wang, H., Yang, H., Xu, Y., 2011. Late Quaternary environmental change of Yellow River Basin: an organic geochemical record in Bohai Sea (North China). Org. Geochem. 42, 575–585. http://dx.doi.org/10.1016/j.orggeochem.2011.04.011.

Tierney, J.E., Russell, J.M., 2009. Distributions of branched GDGTs in a tropical lake system: implications for lacustrine application of the MBT/CBT paleoproxy. Org. Geochem. 40, 1032–1036. http://dx.doi.org/10.1016/j.orggeochem.2009.04.014.

Tierney, J.E., Schouten, S., Pitcher, A., Hopmans, E.C., Sinninghe Damsté, J.S., 2012. Core and intact polar glycerol dialkyl glycerol tetraethers (GDGTs) in Sand Pond, Warwick, Rhode Island (USA): insights into the origin of lacustrine GDGTs. Geochim. Cosmochim. Acta 77, 561–581. http://dx.doi.org/10.1016/j.gca.2011.10.018.

Walsh, E.M., Ingalls, A.E., Keil, R.G., 2008. Sources and transport of terrestrial organic matter in Vancouver Island fjords and the Vancouver-Washington Margin: a multiproxy approach using δ^{13}Corg, lignin phenols, and the ether lipid BIT index. Limnol. Oceanogr. 53, 1054–1063. http://dx.doi.org/10.4319/lo.2008.53.3.1054.

Wang, H., Yang, Z., Saito, Y., Liu, J.P., Sun, X., Wang, Y., 2007. Stepwise decreases of the Huanghe (Yellow River) sediment load (1950–2005): impacts of climate change and human activities. Glob. Planet. Change 57, 331–354. http://dx.doi.org/10.1016/j.gloplacha.2007.01.003.

Wang, H., Liu, W., Zhang, C.L., Wang, Z., Wang, J., Liu, Z., et al., 2012. Distribution of glycerol dialkyl glycerol tetraethers in surface sediments of Lake Qinghai and surrounding soil. Org. Geochem. 47, 78–87. http://dx.doi.org/10.1016/j.orggeochem.2012.03.008.

Weijers, J.W.H., Schouten, S., Spaargaren, O.C., Sinninghe Damsté, J.S., 2006a. Occurrence and distribution of tetraether membrane lipids in soils: implications for the use of the TEX86 proxy and the BIT index. Org. Geochem. 37, 1680–1693. http://dx.doi.org/10.1016/j.orggeochem.2006.07.018.

Weijers, J.W.H., Schouten, S., Hopmans, E.C., Geenevasen, J.A.J., David, O.R.P., Coleman, J.M., et al., 2006b. Membrane lipids of mesophilic anaerobic bacteria thriving in peats have typical archaeal traits. Environ. Microbiol. 8, 648–657. http://dx.doi.org/10.1111/j.1462-2920.2005.00941.x.

Weijers, J.W.H., Schouten, S., van den Donker, J.C., Hopmans, E.C., Sinninghe Damsté, J.S., 2007a. Environmental controls on bacterial tetraether membrane lipid distribution in soils. Geochim. Cosmochim. Acta 71, 703–713. http://dx.doi.org/10.1016/j.gca.2006.10.003.

Weijers, J.W.H., Schefuß, E., Schouten, S., Sinninghe Damsté, J.S., 2007b. Coupled thermal and hydrological evolution of tropical Africa over the last deglaciation. Science 315, 1701–1704. http://dx.doi.org/10.1126/science.1138131.

Wu, W., Zhao, L., Pei, Y., Ding, W., Yang, H., Xu, Y., 2013. Variability of tetraether lipids in Yellow River-dominated continental margin during the past eight decades: implications for organic matter sources and river channel shifts. Org. Geochem. 60, 33–39. http://dx.doi.org/10.1016/j.orggeochem.2013.04.014.

Xie, S., Pancost, R.D., Chen, L., Evershed, R.P., Yang, H., Zhang, K., et al., 2012. Microbial lipid records of highly alkaline deposits and enhanced aridity associated with significant uplift of the Tibetan Plateau in the Late Miocene. Geology 40, 291–294. http://dx.doi.org/10.1130/g32570.1.

Xu, M., Zhao, Y., Liu, G., Wilson, G.V., 2006. Identification of soil quality factors and indicators for the Loess Plateau of China. Soil Sci. 171, 400–413.

Yang, H., Ding, W.H., Wang, J.X., Jin, C.S., He, G.Q., Qin, Y.M., et al., 2012. Soil pH impact on microbial tetraether lipids and terrestrial input index (BIT) in China. Sci. China — Earth Sci. 55, 236–245. http://dx.doi.org/10.1007/s11430-011-4295-x.

Yang, G., Zhang, C.L., Xie, S., Chen, Z., Gao, M., Ge, Z., et al., 2013. Microbial glycerol dialkyl glycerol tetraethers from river water and soil near the Three Gorges Dam on the Yangtze River. Org. Geochem. 56, 40–50. http://dx.doi.org/10.1016/j.orggeochem.2012.11.014.

Zell, C., Kim, J.-H., Moreira-Turcq, P., Abril, G., Hopmans, E.C., Bonnet, M.-P., et al., 2013. Disentangling the origins of branched tetraether lipids and crenarchaeol in the lower Amazon River: implications for GDGT-based proxies. Limnol. Oceanogr. 58, 343–353. http://dx.doi.org/10.4319/lo.2013.58.1.0343.

Zhang, X., Zhang, Y., Sun, H., Xia, D., 2006. Changes of hydrological environment and their influences on coastal wetlands in the southern Laizhou Bay, China. Environ. Monit. Assess. 119, 97–106. http://dx.doi.org/10.1007/s10661-005-9012-9.

Zhao, M., Gao, W., Xing, L., Zhang, Y., Li, L., Liu, J., 2011. Estimates of the origins of organic matter in the Old-Huanghe estuary using the BIT index. Mar. Geol. Quat. Geol. 31, 29–37. http://dx.doi.org/10.3724/SP.J.1140.2011.04029 (in Chinese).

Zhu, C., Weijers, J.W.H., Wagner, T., Pan, J.-M., Chen, J.-F., Pancost, R.D., 2011. Sources and distributions of tetraether lipids in surface sediments across a large river-dominated continental margin. Org. Geochem. 42, 376–386. http://dx.doi.org/10.1016/j.orggeochem.2011.02.002.